NUMERICAL SIMULATION OF FLUID FLOWS IN PETROLEUM RESERVOIRS USING A CELL CENTERED NON-LINEAR FINITE VOLUME METHOD IN UN-STRUCTURED POLYGONAL MESHES

[1]Contreras Fernando RL

[2]Souza Marcio RA

ferlicapac@gmail.com

souza2105@gmail.com

[3]Lyra Paulo RM

[4]Carvalho Darlan KE

prmlyra@padmec.org

dkarlo@oul.com.br

[1,3,4]*Department of Mechanical Engineering, UFPE,* Av. Acadêmico Hélio Ramos s/n, CEP: 50670-901, Pernambuco, Recife, Brazil.. [2]*Department of Renewable Energy Engineering, UFPB,* BR 230, km 21 s/n, CEP: 58059-900, João Pessoa, PB, Brazil

Abstract. The adequate numerical approximation of the equations that describe the incompressible fluid flow in petroleum reservoirs represents a great challenge from a numerical point of view. In fact, for the elliptic pressure equation the permeability tensor can be highly anisotropic, and, as far as the authors know, no linear convergent scheme can guarantee monotone solutions for any polygonal mesh or high anisotropy ratio, producing spurious oscillations for the pressure variable. Besides, the non-linear hyperbolic character of the saturation equation may lead to the formation of saturation shocks even when the initial saturation distribution is smooth throughout the reservoir. In general, the system of equations that describes the fluid flow in petroleum reservoirs can be solved by an IMPES (Implicit Pressure Explicit Saturation) procedure, in which the pressure field is solved implicitly and the saturation field is computed explicitly. In the present work, to solve the pressure equation, we use a Non-Linear Finite Volume method that satisfies the Linearity-Preserving (LP) criterion and produces monotone solution on any star-shaped polygonal meshes and arbitrary anisotropic permeability tensors (NLFV). To solve the saturation equation, we use a multidimensional 2nd order MUSCL type finite volume method (HOMFV) to reduce the artificial numerical diffusion and the Grid Orientation Effect (GOE). To show the potential of our finite volume formulation, we solve some benchmark problems found in literature.

Keywords: *Oil-Water Displacements, Numerical Simulation, Non-Linear Monotone Finite Volume, MUSCL.*

1 INTRODUCTION

The equations that describe the two-phase flow of oil and water in oil reservoirs have an elliptic operator with a diffusion coefficient, which is in general heterogeneous and possibly discontinuous full tensor. This fact suggests the use of robust formulations, with expressions for the fluxes that adequately represent the heterogeneity and anisotropy typical of oil reservoirs. The numerical simulation of these processes requires more accurate and reliable discretization methods. In fact, according to (Lipnikov et al, 2007; Sheng and Yuan, 2008; Gao and Wu, 2013) an "ideal" numerical discretization method for the discretization of diffusion type equation, such as the pressure equation, should satisfy the following criteria: be locally conservative; be monotone, preserve positive solutions whenever is the case or even satisfy the Discrete Maximum Principle (DMP), satisfy the linearity-preserving criterion, i.e., lead to symmetric and positive definite linear systems, and be at least second order accurate for general polygonal meshes and in the presence of full tensors. In the context of petroleum reservoir simulation, failure to satisfy the DMP or at least failure to produce monotone solutions leads to spurious oscillations in the pressure field that can, for instance, lead to the appearance of spurious gas in regions of the reservoir where the pressure falls erroneously below the bubble point. Besides these pressure fields are associated with non-physical Darcy velocities. Is worth remembering that, in linear cases the monotonicity requirement is equivalent to the DMP. However, for general cases, the discrete maximum principle is more restrictive than monotonicity (Sheng and Yuan, 2011; Gao and Wu, 2013). In recent years different nonlinear finite volume methods have been proposed in literature (Le Potier, 2005; Lipnikov et al., 2007; Sheng and Yuan, 2008; Sheng and Yuan, 2011, Gao and Wu, 2013). Some of them formally guarantee monotonicity (in the sense of preserving positive solutions) and other satisfy the Discrete Maximum Principle (DMP), even for problems involving heterogeneous, possibly discontinuous diffusion tensors with high anisotropy ratios in general polygonal meshes (Sheng and Yuan, 2011; Gao and Wu, 2013). In the present paper, in order to solve the elliptic pressure equation, we have devised and implemented a full locally conservative formulation using a IMPES (Implicit Pressure Explicit Saturation) procedure in which the pressure equation is solved by means of a Non-Linear Finite Volume method originally proposed by (Sheng and Yuan, 2008), with a different explicit weight linear preserving interpolant. This method provides monotone solutions and it reproduces piecewise linear solutions exactly even for very distorted meshes and arbitrary anisotropic reservoirs. For the discretization of the saturation equation we devised a cell centered MUSCL-type (Monotone Upstream Centered Scheme for Conservation Laws) method that also guarantees that the saturation field satisfies the DMP criteria. In order to validate the proposed methodology, we solve a benchmark problem found in literature.

2 MATHEMATICAL FORMULATION

In this section, we briefly present the equations that describe the oil and water displacement within the petroleum reservoir. As basic hypothesis we assume that the flow is isothermal and the porous medium and fluid are both incompressible, furthermore, without loss generality, we neglect the capillary and gravitational effects. The equations are derived from Darcy's law and the conservation of mass for each phase. The two phases are denoted by subscripts $\alpha = w, o$ whereby "w" refers to water (wetting phase) "o" refers to oil (non-wetting phase).

$$\frac{\partial\left(\phi\rho_\alpha S_\alpha\right)}{\partial t} = -\nabla\cdot\left(\rho_\alpha\vec{v}_\alpha\right) + q_\alpha, \quad \alpha = w, o \tag{1}$$

and Darcy's law

$$\vec{v}_\alpha = -\lambda_\alpha \underset{\sim}{K}\nabla p_\alpha, \ \alpha = o, w \tag{2}$$

In Equations (1) and (2), ϕ is the rock porosity, ρ_α and S_α, represent the density and the saturation of phase α, respectively. Furthermore, $\vec{v}_\alpha$ is the Darcy's phase velocity and q_α denotes source or sink terms (e.g., injection or production wells) and $\underset{\sim}{K}$ is the absolute rock permeability tensor, which satisfies the ellipticity condition. The fluid mobility term is given by $\lambda_\alpha = k_{r\alpha}/\mu_\alpha$, where μ_α and $k_{r\alpha}\left(S_\alpha\right)$ represent the viscosity and the relative permeability of phase α, respectively.

We also assume that the porous medium is fully saturated by oil and water. Then, due to this last auxiliary hypothesis, we can write:

$$S_o + S_w = 1 \tag{3}$$

By using equations (1) to (3) and after some algebraic manipulation (Aziz, 1979; Carvalho et al., 2006), we can write the elliptic pressure equation, as:

$$\nabla\cdot\vec{v} = Q \text{ with } \vec{v} = -\lambda\underset{\sim}{K}\nabla p \tag{4}$$

In which the total mobility λ is given by:

$$\lambda = \lambda_o + \lambda_w \tag{5}$$

In Equation (4) the total fluid velocity is denoted by $\vec{v} = \vec{v}_w + \vec{v}_o$. The total fluid injection or production specific rate is denoted by $Q = Q_w + Q_o$ with $Q_\alpha = q_\alpha/\rho_\alpha$. Again, by using Eqs. (1) to (3) and after some algebraic manipulation (Aziz, 1979; Carvalho et al., 2006), we can write the hyperbolic saturation equation, as:

$$\phi\frac{\partial S_w}{\partial t} = -\nabla\cdot\vec{F}(S_w) + Q_w \tag{6}$$

In Equation (6), the flux function is defined by $\vec{F}(S_w) = f\left(S_w\right)\vec{v} = f_w\vec{v}$ where $f\left(S_w\right) = \lambda_w/\lambda$ is the fractional flow of water, which is a non-linear function of the water-phase saturation.

1.1 Initial and boundary conditions

The problem described by Equations (4) and (6) is only completely determined when we use an appropriate set of initial and boundary conditions. Typical boundary and initial conditions are given by (Aziz, 1979):

$$
\begin{aligned}
&p(\vec{x},t) = g_D \quad on \quad \Gamma_D \times [0,t], \\
&\vec{v}\cdot\vec{n} = g_N \quad on \quad \Gamma_N \times [0,t], \\
&S_w(\vec{x},t) = \bar{S}_w \quad on \quad \Gamma_I \times [0,t], \\
&S_w(\vec{x},0) = \bar{S}_w^0 \quad on \quad \Omega
\end{aligned}
\tag{7}
$$

where Γ_D and Γ_N represent the Dirichlet and Neumann boundary conditions, respectively, and Γ_I represents injection wells. The scalar function g_D (prescribed pressures) is defined in Γ_D and g_N (prescribed fluxes) is defined in Γ_N, $\bar{S}_w$ represents the prescribed water saturation in a set of injection wells and, finally, $\bar{S}_w^0$ is the initial saturation distribution throughout the domain Ω.

3 NUMERICAL FORMULATION

As previously mentioned, the pressure and the saturation equations are sequentially solved in an IMPES procedure. In this formulation, given an initial distribution of saturation of fluids within the reservoir, we calculate the pressure field implicitly, then we compute the velocity field which is used as an input for the explicit computation of the saturation field. The process is repeated until the end of the simulation is achieved. The main advantages of the IMPES methodology are its simplicity of implementation and its low computational cost for each time step, even though, depending on the complexity of the problem the time step restriction associated to the CFL condition may be too severe, turning this method unfeasible for many practical applications.

3.1 Implicit pressure equation

Let Ω the computational domain connected over $\mathbb{R}^2$ and limited by the contour $\partial\Omega = \Gamma_D \cup \Gamma_N$ and $\Gamma_D \cap \Gamma_N = \{\}$. The computational domain is discretized by a finite set of polygons called control volumes (CV) denoted by $\hat{L}$ or $\hat{R}$, where to each barycenter of the CV ($\hat{L}$) we associate a colocation point that we also denote by $\hat{L}$, even though other colocation points can be used (Le Potier, 2005; Lipnikov at al., 2007). Furthermore, we assume that each polygon is star-shaped with respect to the colocation point (Gao and Wu, 2013; Wu and Gao, 2014; Gao and Wu, 2015).

Integrating Equation (4) over each control volume of the computational domain and using the divergence theorem, for a particular CV, we can write:

$$
\int_{\partial\hat{L}} -\underset{\sim}{K}\nabla p\cdot\vec{n}\, d\Gamma = \int_{\partial\hat{L}} \vec{v}\cdot\vec{n}\, d\Gamma = \int_{\hat{L}} Q\, dV \tag{8}
$$

where $\vec{n}$ the outward unit is vector normal the boundary $\partial\hat{L}$ and Q is the volumetric source term. Using the mean value theorem and after some algebraic manipulation, we obtain the discretized of the form of Eq. (8), as:

$$\sum_{IJ\in\partial\hat{L}} \vec{v}_{IJ}\cdot\vec{N}_{IJ} = \bar{Q}V_{\hat{L}} \text{ where } \vec{v}_{IJ} = \frac{1}{\left|\overrightarrow{IJ}\right|}\int_{IJ\in\partial\hat{L}} \vec{v}\,d\Gamma \text{ and } \bar{Q} = \frac{1}{\left|V_{\hat{L}}\right|}\int_{\hat{L}} Q dV \tag{9}$$

where $\vec{N}_{IJ}$ is the normal vector to edge $\overrightarrow{IJ}$ with $\left|\vec{N}_{IJ}\right| = \left|\overrightarrow{IJ}\right|$, in Eq. (9), the flux density, $\vec{v}_{IJ}\cdot\vec{N}_{IJ}$, can be discretized in many ways, each one leading to a different linear or non-linear finite volume scheme (Lipnikov et al., 2007; Le Potier, 2005; Sheng and Yuan, 2008; Gao and Wu, 2013; Aavatsmark et al., 2002; Gao an Wu; 2010; Lamine and Edwards, 2010). In the present work, we use a Non-Linear Finite Volume method that satisfies various numerical properties that are particularly important in the petroleum reservoir simulation context as it is locally conservative and monotone over any star-shaped polygonal meshes and for arbitrary permeability tensors.

Before describing the discretized flux $\vec{v}_{IJ}\cdot\vec{N}_{IJ}$, we define various physical and geometrical parameters, as the angle formed by segment $\overrightarrow{\hat{L}T}$ (or $\overrightarrow{\hat{L}I}$) and the co-normal $\underset{\sim}{K}_{\hat{L}}\vec{n}_{IJ}$ is denoted by $\theta_{\hat{L},1}$ (or $\theta_{\hat{L},2}$), where $\theta_{\hat{L},1}, \theta_{\hat{L},2} < \pi$ and $\theta_{\hat{L},1} + \theta_{\hat{L},2} < \pi$ (see figure 1). From these assumptions, we can define the following identity:

$$\underset{\sim}{K}_{\hat{L}}\vec{n}_{IJ} = \zeta\left(I - \hat{L}\right) + \xi\left(T - \hat{L}\right) \tag{10}$$

where

$$\zeta = \frac{\left|\underset{\sim}{K}_{\hat{L}}\vec{n}_{IJ}\right|\sin(\theta_{\hat{L},1})}{\left|\overrightarrow{\hat{L}I}\right|\sin(\theta_{\hat{L},1}+\theta_{\hat{L},2})} \text{ and } \xi = \frac{\left|\underset{\sim}{K}_{\hat{L}}\vec{n}_{IJ}\right|\sin(\theta_{\hat{L},2})}{\left|\overrightarrow{\hat{L}T}\right|\sin(\theta_{\hat{L},1}+\theta_{\hat{L},2})} \tag{11}$$

It is important to note that in order to obtain a monotone non-linear finite volume method it is necessary that the coefficients ζ, ξ are non-negatives (Sheng and Yuang, 2008; Sheng and Yuan, 2011; Gao and Wu, 2013; Wu and Gao, 2014; Gao and Wu, 2015).

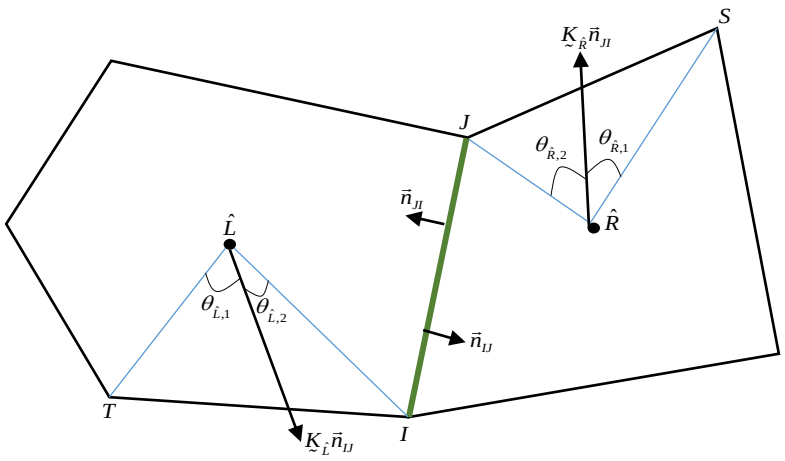

Figure 1. Representation of the physical-geometric parameters.

3.1.1 Construction of the one-sided flux.

Multiplying the identity, Eq. (10), by the pressure gradient and integrating over the edge $\overrightarrow{IJ}$, after some algebraic manipulation we derived the one-side flux density formula, as:

$$\vec{v}_{IJ}^{\hat{L}} \cdot \vec{N}_{IJ} = \lambda_{IJ} \left[\zeta_{IJ,\hat{L}} \left(p_{\hat{L}} - p_T \right) + \xi_{IJ,\hat{L}} \left(p_{\hat{L}} - p_I \right) \right] \tag{12}$$

and

$$\vec{v}_{IJ}^{\hat{R}} \cdot \vec{N}_{JI} = \lambda_{IJ} \left[\zeta_{IJ,\hat{R}} \left(p_{\hat{R}} - p_J \right) + \xi_{IJ,\hat{R}} \left(p_{\hat{R}} - p_S \right) \right] \tag{13}$$

In equations (12) and (13), $p_{\hat{R}}$, $p_{\hat{L}}$ are the primary variables and p_I, p_J, p_T and p_S are interpolated as a linear combination of the surrounding cell-centered unknowns, reducing the scheme to a completely cell-centered one. The weights of the linear combination are obtained explicitly, without any other local inversion process that is common to other cell centered finite volume methods (Gao and Wu, 2010; Queiroz et al., 2014). Furthermore, mid-edge mobilities λ_{IJ} are obtained by using the arithmetic average of the nodal mobilities which are computed as:

$$\lambda_j = \sum_{k=1}^{ncv_j} \lambda_{\hat{k}} V_{\hat{k}} \Bigg/ \sum_{k=1}^{ncv_j} V_{\hat{k}}, \quad j = I, J \tag{14}$$

here, $\lambda_{\hat{k}}$ is the total mobility of each control volume surrounding node j and ncv_j is the number of control volumes surrounding that node.

Having the one-sided fluxes in Eq. (12), (13) we can to define the unique flux on edge $\overrightarrow{IJ}$ as the linear combinations of these $\vec{v}_{IJ}^{\hat{L}} \cdot \vec{N}_{IJ}$, $\vec{v}_{IJ}^{\hat{R}} \cdot \vec{N}_{IJ}$ i.e.

$$\vec{v}_{IJ} \cdot \vec{N}_{IJ} = \mathfrak{W}_{IJ,\hat{L}} \vec{v}_{IJ}^{\hat{L}} \cdot \vec{N}_{IJ} - \mathfrak{W}_{IJ,\hat{R}} \vec{v}_{IJ}^{\hat{R}} \cdot \vec{N}_{JI} \tag{15}$$

where $\mathfrak{W}_{IJ,\hat{L}}$, $\mathfrak{W}_{IJ,\hat{R}}$ are two positive parameters, satisfying

$$\mathfrak{W}_{IJ,\hat{L}} + \mathfrak{W}_{IJ,\hat{R}} = 1 \tag{16}$$

Besides, the finite volume method is locally conservative, since for any edge $\overrightarrow{IJ}$ separating $\hat{L}$ and $\hat{R}$, one has

$$\vec{v}_{IJ} \cdot \vec{N}_{IJ} + \vec{v}_{IJ} \cdot \vec{N}_{JI} = 0 \tag{17}$$

Substituting the Eqs. (12) and (13) in (15), we have:

$$\begin{aligned}\vec{v}_{IJ}\cdot\vec{N}_{IJ} = {} & \lambda_{IJ}\,\mathfrak{W}_{IJ,\hat{L}}\left(\zeta_{IJ,\hat{L}}+\xi_{IJ,\hat{L}}\right)p_{\hat{L}} - \lambda_{IJ}\,\mathfrak{W}_{IJ,\hat{R}}\left(\zeta_{IJ,\hat{R}}+\xi_{IJ,\hat{R}}\right)p_{\hat{R}} + \ldots \\ & \lambda_{IJ}\,\mathfrak{W}_{IJ,\hat{R}}\left(\zeta_{IJ,\hat{R}}\,p_J+\xi_{IJ,\hat{R}}\,p_S\right) - \lambda_{IJ}\,\mathfrak{W}_{IJ,\hat{L}}\left(\zeta_{IJ,\hat{L}}\,p_T+\xi_{IJ,\hat{L}}\,p_I\right)\end{aligned} \tag{18}$$

In order to obtain a non-linear finite volume method based on two-point flux approximation, the third and four terms of Eq. (18) should vanish, so

$$\begin{cases}\lambda_{IJ}\,\mathfrak{W}_{IJ,\hat{R}}\left(\zeta_{IJ,\hat{R}}\,p_J+\xi_{IJ,\hat{R}}\,p_S\right) - \lambda_{IJ}\,\mathfrak{W}_{IJ,\hat{L}}\left(\zeta_{IJ,\hat{L}}\,p_T+\xi_{IJ,\hat{L}}\,p_I\right)=0 \\ \mathfrak{W}_{IJ,\hat{L}}+\mathfrak{W}_{IJ,\hat{R}}=1\end{cases} \tag{19}$$

After algebraic manipulation of the system of equations (19), the parameters $\mathfrak{W}_{IJ,\hat{L}}$ and $\mathfrak{W}_{IJ,\hat{R}}$ are given by

$$\mathfrak{W}_{IJ,\hat{L}}=\frac{\left|a_{IJ}^{\hat{R}}\right|+\varepsilon}{\left|a_{IJ}^{\hat{R}}\right|+\left|a_{IJ}^{\hat{L}}\right|+2\varepsilon} \text{ and } \mathfrak{W}_{IJ,\hat{R}}=\frac{\left|a_{IJ}^{\hat{L}}\right|+\varepsilon}{\left|a_{IJ}^{\hat{R}}\right|+\left|a_{IJ}^{\hat{L}}\right|+2\varepsilon} \tag{20}$$

In which $a_{IJ}^{\hat{L}}=\zeta_{IJ,\hat{L}}\,p_T+\xi_{IJ,\hat{L}}\,p_I$, $a_{IJ}^{\hat{R}}=\zeta_{IJ,\hat{R}}\,p_J+\xi_{IJ,\hat{R}}\,p_S$ and $\varepsilon=1\mathrm{E}-16$.

Considering Eq. (19) in Eq. (18), we defined the unique flux on the edge $\overrightarrow{IJ}$, as:

$$\vec{v}_{IJ}\cdot\vec{N}_{IJ}=A_{IJ}^{\hat{L}}(p)\,p_{\hat{L}}-A_{IJ}^{\hat{R}}(p)\,p_{\hat{R}} \tag{21}$$

where $A_{IJ}^{\hat{L}}(p)=\lambda_{IJ}\,\mathfrak{W}_{IJ,\hat{L}}\left(\zeta_{IJ,\hat{L}}+\xi_{IJ,\hat{L}}\right)$ and $A_{IJ}^{\hat{R}}(p)=\lambda_{IJ}\,\mathfrak{W}_{IJ,\hat{R}}\left(\zeta_{IJ,\hat{R}}+\xi_{IJ,\hat{R}}\right)$.

Remembering that the coefficients ζ, ξ in Eq. (11) and the parameters $\mathfrak{W}_{IJ,\hat{L}}$, $\mathfrak{W}_{IJ,\hat{R}}$ in Eq. (20) are nonnegative real numbers, furthermore, the mid-edge mobility λ_{IJ}, due to the definition of relative permeability, is a nonnegative value, then $A_{IJ}^{\hat{L}}(p)\geq 0$ and $A_{IJ}^{\hat{R}}(p)\geq 0$. This condition is fundamental to guarantee that the method is monotone.

Whenever, $IJ\in\partial\Omega\cap\hat{L}$, i.e., the control surface lies over the boundary, the flux density can be directly computed, by:

$$\vec{v}_{IJ}^{\hat{L}}\cdot\vec{N}_{IJ}=A_{IJ}^{\hat{L}}(p)\,p_{\hat{L}}-a_{IJ}^{\hat{L}} \tag{22}$$

where $A_{IJ}^{\hat{L}}(p)=\lambda_{IJ}\,\mathfrak{W}_{IJ,\hat{L}}\left(\zeta_{IJ,\hat{L}}+\xi_{IJ,\hat{L}}\right)$ and $a_{IJ}^{\hat{L}}=\lambda_{IJ}\left(\zeta_{IJ,\hat{L}}\,p_T+\xi_{IJ,\hat{L}}\,p_I\right)$.

3.1.2. Interpolating pressures on mesh nodes.

As previously mentioned, pressures on mesh vertices are written as linear weighted combinations of the neighboring cell-centered unknowns i.e.:

$$p_I = \sum_{i=1}^{ncv} w_{\hat{i}}\, p_{\hat{i}} \tag{23}$$

where $w_{\hat{i}}$ is the weight assigned to each control volume $\hat{i}$.

In the present work, we used one type of explicit weight proposed by (Gao and Wu, 2010). This weight is called "explicit" to indicate that it is computed without the need of solve a set of local system of equations, as in others classic MPFA methods (Aavatsmark, 2002). However, the LPEW interpolation the explicit weight in Eq. (23) is derived using the continuity equation throughout the auxiliary "interaction regions" built around each mesh vertex. In figure 2, we present the interaction regions and some geometric parameters for the LPEW interpolation, following (Gao and Wu, 2010), the explicit weights can be computed as:

$$w_{\hat{i}} = \bar{\varpi}_{\hat{i}} \Big/ \sum_{i}^{ncv} \bar{\varpi}_{\hat{i}}\,, \quad \hat{i} = 1, 2, ..., ncv \tag{24}$$

In equation (24), the coefficients $\bar{\varpi}_{\hat{i}}$ are given by:

$$\bar{\varpi}_{\hat{i}} = K^{(n)}_{\hat{i},1}\eta_{\hat{i},1}\xi\left(\hat{i}\right) + \xi\left(\hat{i}+1\right)K^{(n)}_{\hat{i},2}\eta_{\hat{i},2} \text{ and } \xi\left(\hat{i}\right) = \lambda_{\hat{i}}\kappa_{\hat{i}} + \lambda_{\hat{i}-1}\kappa_{\hat{i}-1} \tag{25}$$

where $\lambda_{\hat{i}}$ is the total mobility for each control volume $\Omega_{\hat{i}}$, $\eta_{\hat{i},1}$, $\eta_{\hat{i},2}$ are given by:

$$\eta_{\hat{i},1} = \left|\overrightarrow{I\bar{M}_i}\right| \Big/ h^{\hat{i}}_{IJ_i}\,, \quad \eta_{\hat{i},2} = \left|\overrightarrow{I\bar{M}_{i+1}}\right| \Big/ h^{\hat{i}}_{IJ_{i+1}} \tag{26}$$

where $\bar{M}$ is middle point of the edge and $h^{\hat{i}}_{IJ_i}$ and $h^{\hat{i}}_{IJ_{i+1}}$ are the distances as presented in Figure 2.

The projections of the permeability tensor of the adjacent control volumes that share edge $\overrightarrow{I\bar{M}_\alpha}$ on the normal (*n*) and tangential (*t*) directions to this edge are given by:

$$K^{(n)}_{\hat{i},k} = \left[\left(\vec{N}_{I\bar{M}_\alpha}\right)^{\mathrm{T}} \underset{\sim}{K}_{\hat{i}} \left(\vec{N}_{I\bar{M}_\alpha}\right)\right] \Big/ \left|\overrightarrow{I\bar{M}_\alpha}\right|^2,\; K^{(t)}_{\hat{i},k} = \left[\left(\vec{N}_{I\bar{M}_\alpha}\right)^{\mathrm{T}} \underset{\sim}{K}_{\hat{i}} \left(\overrightarrow{I\bar{M}_\alpha}\right)\right] \Big/ \left|\overrightarrow{I\bar{M}_\alpha}\right|^2 \tag{27}$$

with, $\alpha = \hat{i} + k - 1$; and k=1,2. Furthermore:

$$\kappa_{\hat{i}} = \frac{\overline{K}^{(n)}_{\hat{i}}\, ctg(\vartheta_{\hat{i},2}) - \overline{K}^{(t)}_{\hat{i}}}{K^{(n)}_{\hat{i}-1,2}\, ctg(\theta_{\hat{i}-1,2}) + K^{(n)}_{\hat{i},1}\, ctg(\theta_{\hat{i},1}) - K^{(t)}_{\hat{i}-1,2} + K^{(t)}_{\hat{i},1}} \tag{28}$$

$$\kappa_{\hat{i}-1} = \frac{\overline{K}^{(n)}_{\hat{i}-1}\, ctg(\vartheta_{\hat{i}-1,1}) + \overline{K}^{(t)}_{\hat{i}-1}}{K^{(n)}_{\hat{i}-1,2}\, ctg(\theta_{\hat{i}-1,2}) + K^{(n)}_{\hat{i},1}\, ctg(\theta_{\hat{i},1}) - K^{(t)}_{\hat{i}-1,2} + K^{(t)}_{\hat{i},1}} \tag{29}$$

where,

$$\overline{K}_{\hat{i}}^{(n)} = \left[\left(\vec{N}_{\bar{M}_i \bar{M}_{i+1}} \right)^{\mathrm{T}} \underset{\sim}{K}_{\hat{i}} \left(\vec{N}_{\bar{M}_i \bar{M}_{i+1}} \right) \right] \Big/ \left| \overrightarrow{\bar{M}_i \bar{M}_{i+1}} \right|^2 \tag{30}$$

$$\overline{K}_{\hat{i}}^{(t)} = \left[\left(\vec{N}_{\bar{M}_i \bar{M}_{i+1}} \right)^{\mathrm{T}} \underset{\sim}{K}_{\hat{i}} \left(\overrightarrow{\bar{M}_i \bar{M}_{i+1}} \right) \right] \Big/ \left| \overrightarrow{\bar{M}_i \bar{M}_{i+1}} \right|^2 \tag{31}$$

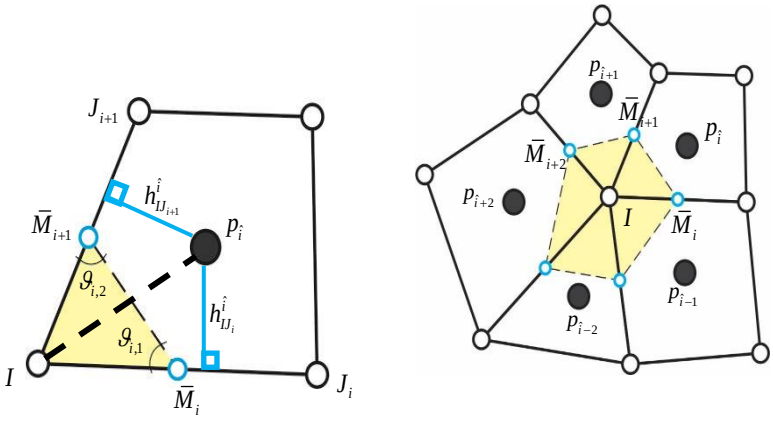

Figure 2. The interaction region for the LPEW interpolation.

Again, the geometric coefficients $\kappa_{\hat{i}}$, $\overline{K}_{\hat{i}}^{(n)}$, $\overline{K}_{\hat{i}}^{(t)}$ are computed during the preprocessing stage and only the mobility terms are updated at each time step. Further details of the LPEW interpolation can be found in (Gao and Wu, 2010; Queiroz et al., 2014).

The weights in Eq. (24) may have negative value ($\omega_{\hat{i}} < 0$), but this leads to no problem referring to the monotonicity of this scheme. In classical methods this interpolation, i.e. LPEW, does not preserve monotonicity (Queiroz et al., 2014), and when that happens the authors suggested to use interpolations methods of lower-order and that are positive-preserving, such as Inverse Distance Weights (IDW) (Le Potier, 2005; Lipnikov et al., 2007; Queiroz et al., 2014). However, the use of this interpolation may lead to poor accuracy in very distorted meshes (Gao and Wu, 2014; Gao and Wu, 2015).

3.1.2 Discrete system.

For every each control volume $\hat{L}$, the discrete pressure equation (9) is

$$\sum_{IJ \in \partial \hat{L}} \vec{v}_{IJ} \cdot \vec{N}_{IJ} = \bar{Q} V_{\hat{L}}, \ \forall \hat{L} \in \Omega \tag{32}$$

We can write the pressure equation, Eq. (9), for all control volumes of the computational mesh in the following matrix form:

$$\underline{\underline{T}}(p)\,\underline{p} = \underline{Q}(p) \tag{33}$$

The transmissibility matrix $\underline{\underline{T}}(P)$ is obtained by the assemble of the following *2 x 2* matrices, which are associated to internal control surfaces (i.e., edges in 2D)

$$\underline{\underline{T}}(p)_{IJ} = \begin{pmatrix} A_{IJ}^{\hat{L}}(p) & -A_{IJ}^{\hat{R}}(p) \\ -A_{IJ}^{\hat{L}}(p) & A_{IJ}^{\hat{R}}(p) \end{pmatrix} \tag{34}$$

and by *(1 X 1)* matrices of the form:

$$\underline{\underline{T}}(p)_{IJ} = A_{IJ}^{\hat{L}} \tag{35}$$

for Dirichlet edges. The right hand side vector $\underline{Q}$ is generated by the source and the boundary data.

The non-linear system of Eq. (33) may be solved by different methods. Following the work of (Lipnikov et al., 2007; Le Potier, 2005; Sheng and Yuan, 2008; Sheng and Yuan, 2011; Gao and Wu, 2013; Gao and Wu, 2014; Gao and Wu, 2015), we use the Picard iteration method, which can be briefly described as follows. Choose a small $\varepsilon_{non} > 0$ and an initial vector p^0 positive and repeat until convergence is reached to the prescribed tolerance ε_{non}, i.e.:

1. Solve $\underline{\underline{T}}\left(p^{k+1}\right)\underline{p}^{k} = \underline{Q}(\mathrm{p}^{k})$
2. Stop if $\left\|\underline{\underline{M}}\left(p^{k+1}\right)\underline{p}^{k+1} - \underline{F}\left(p^{k+1}\right)\right\| \le \varepsilon_{non}\left\|\underline{\underline{M}}\left(p^{0}\right)\underline{p}^{0} - \underline{F}\left(p^{0}\right)\right\|$.

3.2 Explicit saturation equation

In order to obtain the discretized saturation equation, we integrate Eq. (6) over an arbitrary control volume $\hat{L}$ where the control surface is denoted by $\partial\hat{L}$, after to use the divergence theorem, we have:

$$\int_{\hat{L}} \phi \frac{\partial S_w}{\partial t} dV = -\int_{\partial\hat{L}} \vec{F}(S_w)\cdot\vec{n}dA + \int_{\hat{L}} Q dV \tag{36}$$

Where $\vec{F}(S_w) = f\left(S_w\right)\vec{v} = f_w\vec{v}$.

The discrete numerical scheme for the solution of the non-linear hyperbolic saturation equation can be written as:

$$S_w^{n+1} = S_w^n + \frac{\Delta t}{\phi V_{\hat{L}}}\left[\bar{Q}V_{\hat{L}} - \sum_{IJ\in\partial\hat{L}} \vec{F}\left(S_{w,IJ}\right)\cdot\vec{N}_{IJ}\right], \text{ where } \vec{F}\left(S_{w,IJ}\right) = \vec{F}_{IJ} = f_w\left(S_{w,IJ}\right)\vec{v}_{IJ} \tag{37}$$

where superscripts *n* and (*n*+1) denotes physical quantities existing at times t^n and t^{n+1}, respectively and $\Delta t = t^{n+1} - t^n$ is the time step. The source term, which is non-zero only at wells, is approximated as:

$$\bar{Q} = \frac{1}{\left|V_{\hat{L}}\right|}\int_{\hat{L}} Q dV \tag{38}$$

The equation (37) is solved by the IMPES strategy. The hyperbolic flux can be calculated using various schemes, for instance: first order upwind method, truly multidimensional upwind, higher resolution schemes or multidimensional higher resolution scheme. The main goal of higher resolution schemes and truly multidimensional is to reduce numerical diffusion and the grid orientation effect (GOE). GOE phenomena are observed, for instance, when the computational grid is rotated and substantially different numerical solutions are obtained for the same problem. Unfortunately, this anomaly is present in standard oil reservoir simulation (Lamine and Edwards, 2010). In order to avoid undesirable numerical diffusion and the GOE, we describe an extension of higher order Godunov methods (MUSCL-type) based in (Hirsch, 1990; Lönher, 2008).

A first order approximation for the advective flux term in the right hand side of the Eq. (38) can be written as:

$$\int_{\Gamma_{\hat{k}}} \vec{F}\cdot\vec{n}\partial\Gamma_{\hat{k}} \cong \sum_{IJ\in\Gamma_{\hat{k}}} \vec{F}_{IJ}\cdot\vec{N}_{IJ} = \sum_{IJ\in\Gamma_{\hat{k}}} \left(\frac{1}{2}\left(\left(\vec{F}_{IJ}\left(S_{w,\hat{L}}\right)+\vec{F}_{IJ}\left(S_{w,\hat{R}}\right)\right)\cdot\vec{N}_{IJ} - \max_{\hat{R},\hat{L}}\left|\alpha_{IJ}\right|\left(S_{w,\hat{R}}-S_{w,\hat{L}}\right)\right)\right) \tag{39}$$

In Equation (39), $S_{w,\hat{L}}$ and $S_{w,\hat{R}}$ represent the values of the water saturation at the control volumes adjacent to the control surface $\overrightarrow{IJ}$, $\vec{F}_{IJ}^{\hat{L}}$ and $\vec{F}_{IJ}^{\hat{R}}$ are the correspondent fluxes, the term $\max_{\hat{R},\hat{L}}\left|\alpha_{IJ}\right|\left(S_{w,\hat{R}}-S_{w,\hat{L}}\right)$ corresponds to the artificial dissipation needed to stabilize the original central scheme, and the wave velocity at the control surface is approximated by:

$$\alpha_{IJ} = \left(\vec{v}_{IJ}\cdot\vec{N}_{IJ}\right)\frac{\partial f}{\partial S} \tag{40}$$

where the fractional flux f is defined in Eq. (6) and $\vec{v}_{IJ}\cdot\vec{N}_{IJ}$ is approximated as given in Eq. (15).

3.3 Reconstruction

The flux approximation of Eq. (39) assumes that, at each time step, the saturation values are constant throughout the CV, producing solutions that are monotone but only first order accurate in space and is called First Order Upwind (FOU) method. In order to obtain a second order approximation, we employ a piecewise linear reconstruction procedure (Hirsch, 1990; Lönher, 2008). Therefore, our upwind-biased linearly reconstructed saturations, $S_{w,\hat{L}}^{+}$ and $S_{w,\hat{R}}^{-}$, are computed as:

$$S_{w,\hat{L}}^{+} = S_{w,\hat{L}} + \frac{\psi_{\hat{L}}^{*}}{6}\left(2\overrightarrow{\hat{L}\hat{R}}\cdot\nabla S_{w,\hat{L}} + \left(S_{w,\hat{R}}-S_{w,\hat{L}}\right)\right), \text{ where } \psi_{\hat{L}}^{*} = \psi_{\hat{L}}\psi_{IJ,\hat{L}} \tag{41}$$

$$S^{-}_{w,\hat{R}} = S_{w,\hat{R}} - \frac{\psi^{*}_{\hat{R}}}{6}\left(2\overrightarrow{\hat{L}\hat{R}}\cdot\nabla S_{w,\hat{R}} + \left(S_{w,\hat{R}} - S_{w,\hat{L}}\right)\right), \text{ where } \psi^{*}_{\hat{R}} = \psi_{\hat{R}}\psi_{IJ,\hat{R}} \tag{42}$$

where, $\nabla S_{w,\hat{L}}$ and $\nabla S_{w,\hat{R}}$ denote the reconstructed gradients defined with respect to the left and right side control volumes, respectively.

Following Blazek (Blazek,2001), the gradients are calculated by a least squares reconstruction. This reconstruction is based upon the use of a Taylor series expansion for each adjacent control volume connected to the cell $\hat{i}$. Therefore, by using the saturations given by Eqs. (41) and (42), we replace the first order approximation of Eq. (39) by its higher order counterpart, which can be written as:

$$\sum_{IJ\in\Gamma_{\hat{k}}} \vec{F}_{IJ}\cdot\vec{N}_{IJ} = \sum_{IJ\in\Gamma_{\hat{k}}}\left(\frac{1}{2}\left(\left(\vec{F}_{IJ}\left(S^{+}_{w,\hat{L}}\right) + \vec{F}_{IJ}\left(S^{-}_{w,\hat{R}}\right)\right)\cdot\vec{N}_{IJ} - \alpha^{-+}_{IJ}\left(S^{-}_{w,\hat{R}} - S^{+}_{w,\hat{L}}\right)\right)\right) \tag{43}$$

In Equations (41) and (42), $\psi^{*}_{\hat{i}}$ is a function that must switch smoothly from one (higher-order scheme) to zero (first order scheme) in the vicinity of saturation shocks, $\psi^{\hat{i}}_{IJ}$ is responsible for the face (edge in 2-D) interpolative boundedness, i.e., it guarantees that the extrapolated values of the saturation through the control surfaces remain between $S_{w,\hat{L}}$ and $S_{w,\hat{R}}$, and the function $\psi^{*}_{\hat{i}}$, is responsible for switching the scheme to first order whenever necessary to guarantee monotonicity, more details in (Woodfield, 2004).

$$\psi_{\hat{i}} = \begin{cases} 1 & \text{if } \left(S_{w,\max} - S_{w,\min}\right) \le 10^{-20} \\ 0 & \text{if } \gamma_{\hat{i}} \ge 1 \text{ or } \gamma_{\hat{i}} \le 0 \\ 1 & \text{if } \delta \le \gamma_{\hat{i}} \le (1-\delta) \\ \gamma_{\hat{i}}/\delta & \text{if } 0 < \gamma_{\hat{i}} < \delta \\ \left(1-\gamma_{\hat{i}}\right)/\delta & \text{if } (1-\delta) < \gamma_{\hat{i}} < 1 \end{cases} \tag{44}$$

The parameter $\gamma_{\hat{i}}$ is defined as:

$$\gamma_{\hat{i}} = \frac{S_{w,\hat{i}} - S_{w,\min}}{S_{w,\max} - S_{w,\min}} \tag{45}$$

In Equations (44) and (45), $S_{w,\max}$ and $S_{w,\min}$ are the maximum and minimum values of the saturation, considering all control volumes that are immediate neighbors of the control volume $\hat{i}$ (i.e., those which share a common control surface), excluding $\hat{i}$ itself, and, as a consequence, the denominator express the maximum difference between the saturations of the neighbors of control volume $\hat{i}$ in each time step. In multi-dimensional problems, the satura-

tion is said to be "bounded" for every control volume $\hat{i}$ in the computational domain, if the following relation is true: $0 \le \gamma_{\hat{i}} \le 1$.

The use of the second order scheme in the whole computational domain, except where Eq. (45) applies is not always a safe strategy, because there is not a smooth transition between the second order and the first order schemes. As pointed out by (Woodfield, 2004), a safer approach consists in introducing an user defined free parameter which ranges from $0 \le \delta \le 0.5$, such as:

$$\delta \le \gamma_{\hat{i}} \le 1-\delta \tag{46}$$

It is worth mentioning that the first requirement stated in Eq. (44) avoids division by zero in the definition of $\gamma_{\hat{i}}$. Following the work of (Woodfield, 2004), we have used $\delta = 0.2$ as a good compromise between robustness and accuracy. Note that, smaller values of this parameter (i.e., close to zero) will turn the scheme less diffusive because the limiter will tend to switch on and off more abruptly as δ tends to zero, while larger values of δ will imply in a more diffusive scheme due to the smaller range of values of $\gamma_{\hat{i}}$ for which the second order scheme is used. Finally, in order to guarantee control surface boundedness, we have used the following variation of the Van Albada face limiter (Lönher, 2008):

$$\psi_{IJ,\hat{L}} = \max\left(0,\ \frac{2\left(2\overrightarrow{\hat{L}\hat{R}}\cdot\nabla S_{w,\hat{L}} - \left(S_{w,\hat{R}} - S_{w,\hat{L}}\right)\right)\left(S_{w,\hat{R}} - S_{w,\hat{L}}\right) + \varepsilon}{\left(2\overrightarrow{\hat{L}\hat{R}}\cdot\nabla S_{w,\hat{L}} - \left(S_{w,\hat{R}} - S_{w,\hat{L}}\right)\right)^2 + \left(S_{w,\hat{R}} - S_{w,\hat{L}}\right)^2 + \varepsilon}\right) \tag{47}$$

$$\psi_{IJ,\hat{R}} = \max\left(0,\ \frac{2\left(2\overrightarrow{\hat{L}\hat{R}}\cdot\nabla S_{w,\hat{R}} - \left(S_{w,\hat{R}} - S_{w,\hat{L}}\right)\right)\left(S_{w,\hat{R}} - S_{w,\hat{L}}\right) + \varepsilon}{\left(2\overrightarrow{\hat{L}\hat{R}}\cdot\nabla S_{w,\hat{R}} - \left(S_{w,\hat{R}} - S_{w,\hat{L}}\right)\right)^2 + \left(S_{w,\hat{R}} - S_{w,\hat{L}}\right)^2 + \varepsilon}\right) \tag{48}$$

where ε is a very small parameter used only to avoid division by zero in smooth regions of the flow.

4 NUMERICAL EXPERIMENT

In order to calculate the convergence rates, we define the following norms of errors:

$$\varepsilon_p(h) = \left(\sum_{i=1}^{N} V_i \left\| p_i - \tilde{p}_i \right\|^2\right)^{0.5} \quad \text{and} \quad R_p = \frac{\log\left(\varepsilon_p(h_2)/\varepsilon_p(h_1)\right)}{\log\left(h_2/h_1\right)} \tag{49}$$

Where N is total number of cells in the computational domain, p and $\tilde{p}$ is numerical and analytical solution, respectively. Furthermore h_1, h_2 denote the mesh sizes of the two successive meshes. In all the tests presented here we consider nonlinear convergence when the residual reduces below the tolerance $\varepsilon_{non} = 1.0\text{E}-07$.

4.1 Single phase flow in a domain with a discontinuous anisotropic permeability tensor

In this example the mobility of fluid is consider unitary, the goal of the problem is show the convergence rate of the method, this problem was adapted from (Gao and Wu, 2010). We consider a square unitary, discretized by a set of successively refined grids (see figure 3) and boundary conditions is fully Dirichlet obtained directly from the exact solution given by:

$$\tilde{p}(x,y)=\frac{1}{2}\left[\frac{\sin((1-x)(1-y))}{\sin(1)}+(1-x)^3(1-y)^2\right] \text{ and } g_D=\tilde{p}(x,y),\ \forall(x,y)\in\Gamma_D \tag{50}$$

The permeability tensor is given by:

$$\underset{\sim}{K}=\begin{pmatrix}1.5 & 0.5\\ 0.5 & 1.5\end{pmatrix} \tag{51}$$

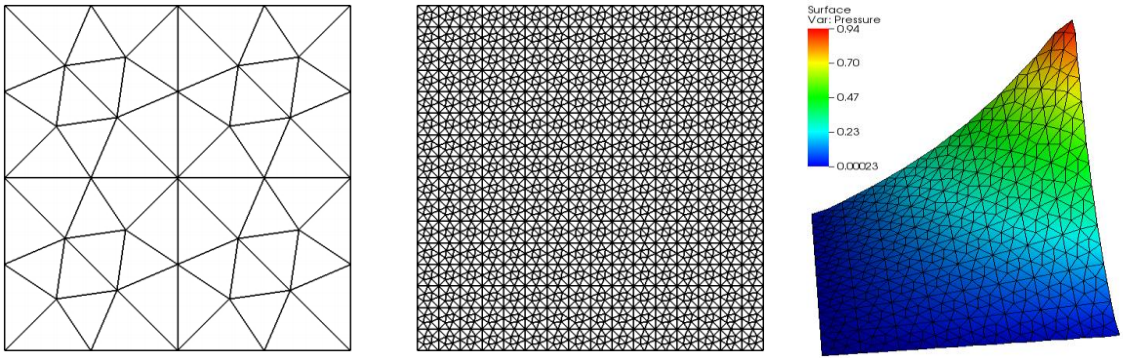

Figure 3. Triangular unstructured coarse and refined meshes and representative numerical solution obtained by NLFV method.

In table 1, we present the errors and convergence rates for successively refined meshes and the number of non-linear iterations for each mesh to achieve convergence.

Table 1. Represent the results convergence for the NLFV scheme.

$1/h$	ε_p	R_p	Iteration
0.25	0.0049	------	11
0.125	0.0012	2.0297	12
0.0625	$3.088\text{x}10^{-4}$	1.9582	15
0.03125	$7.6848\text{x}10^{-5}$	2.0065	18

4.2 One phase flow in a heterogeneous and highly anisotropic domain

In this second problem (Gao and Wu, 2013; Gao and Wu, 2014), we evaluate the performance of the nonlinear finite volume method for a heterogeneous and highly anisotropic oil reservoir, the goal this problem is show that the method satisfies the criterion positive-preserving. We consider a square domain $\Omega = [0,1]^2$ with fully Dirichlet boundary conditions and source term given by:

$$f(x,y) = \begin{cases} \dfrac{81}{4}, \text{if } (x,y) \in \left[\dfrac{7}{18}, \dfrac{11}{18}\right]^2 \\ 0, \qquad \text{otherwise} \end{cases} \quad \text{and } g_D = 0, \ \forall (x,y) \in \Gamma_D \tag{52}$$

In this case, the domain is partitioned in four square subdomains each with a different permeability anisotropic permeability tensor (see figure 4) given by:

$$\underset{\sim}{K} = \begin{pmatrix} \cos(\theta) & -\sin(\theta) \\ \sin(\theta) & \cos(\theta) \end{pmatrix} \begin{pmatrix} 1000 & 0 \\ 0 & 1 \end{pmatrix} \begin{pmatrix} \cos(\theta) & \sin(\theta) \\ -\sin(\theta) & \cos(\theta) \end{pmatrix} \tag{53}$$

For this problem we consider an unstructured quadrilateral mesh with 72x72 control volumes.

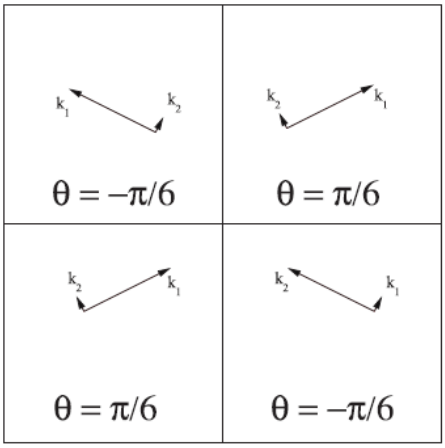

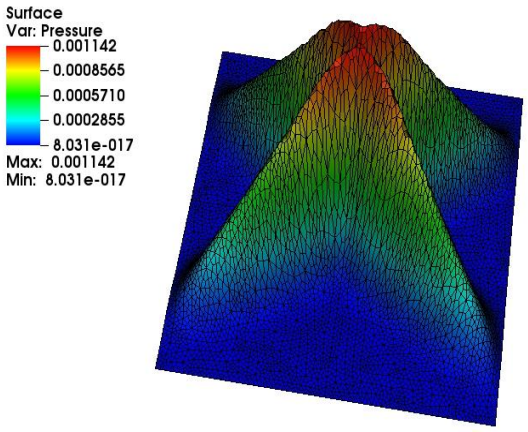

Figure 4. One phase flow in a heterogeneous and highly anisotropic domain: domain configuration and angle of rotation for the permeability tensor (left); Pressure field and triangular mesh (right).

In this case we needed 312 non-linear iterations for convergence and the pressure solution remained positive during the whole process.

4.3 Two-Phase Flow in a ¼ of Five Spot Configuration in a Homogeneous and Anisotropic Reservoir using a Distorted Triangular mesh

This example, adapted from (Lamine and Edwards, 2010), consists in a variation of the classical ¼ of five spot problem, in which we use a full tensor and homogeneous permeability field with principal axes rotated 45 degrees in relation to the square domain, with an anisotropy ratio of $K_{xx}/K_{yy}=10$. The oil and water viscosity ratio is $M\cong(\mu_o/\mu_w)=1$, and the relation between the relative permeabilities is linear with $k_{rw}=S_w$ and $k_{ro}=1-S_w$. In this case, null flux boundary conditions are imposed at all external reservoir boundaries. The water flow rate prescribed at the injection well is one, and pressure is prescribed at the producer with $\overline{p}_{prod}=0$. For comparison purposes we solved this problem using our Non-linear Finite Volume (NLFV) scheme together with the (First Order Upwind) FOU method compared it using the NLFV coupled to our Higher Order MUSCL-Type Finite Volume (HOMFV) method and, as a reference solution, we also solved this problem using the linear MPFA-O method (Aavatsmark, 2002) together with the FOU method using a unstructured quadrilateral mesh with 14988 control volumes. For all methods and mesh configurations we used a CFL number of 0.4.

According to (Lamine and Edwards, 2010), an important feature of this example is the advective transport of a "stable" discontinuity throughout the discretized domain. In Figures 6, we present the saturations profiles obtained using the NLFV method coupled with the FOU scheme (left) and coupled to our HOFVM. Again, it is clear that HOMFV schemes have much less numerical diffusion. In Figure 7, we present the oil recovery and the cumulate oil curves for this problem. In these figures, we observe that the curves obtained by the NLFV coupled with the HOMFV method are much closer to the reference solution than those obtained by the NLFV/FOU method even for this strongly distorted mesh (see Figure 5).

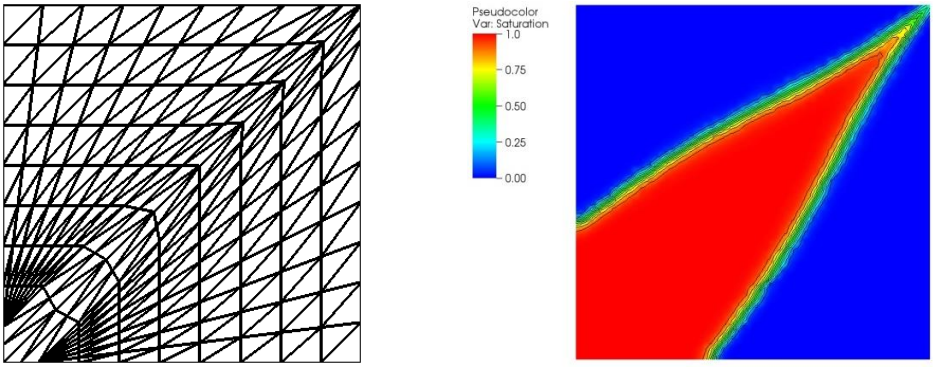

Figure 5. Two-phase flow in a ¼ of five spot configuration in a homogeneous and anisotropic reservoir using a distorted triangular mesh: Computational domain and triangular mesh with 162 control volumes (left); Reference solution at 0.4 PVI obtained for a unstructured quadrilateral mesh with 14,988 control volumes (right).

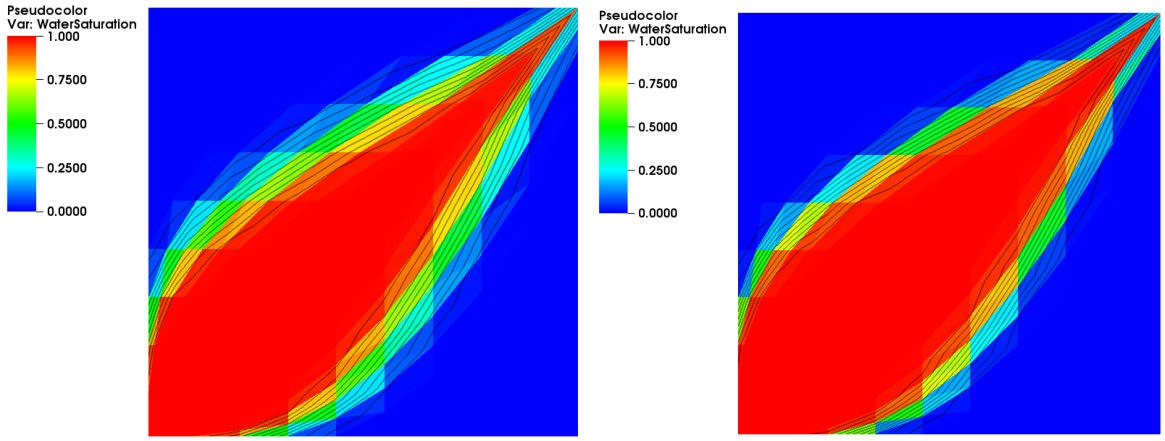

Figure 6. Two-phase flow in a ¼ of five spot configuration in a homogeneous and anisotropic reservoir using a distorted triangular mesh: Saturation profiles obtained with three different methods at t=0.25 PVI: (a) NLFV/FOU; (b) NLFV/HOMFV.

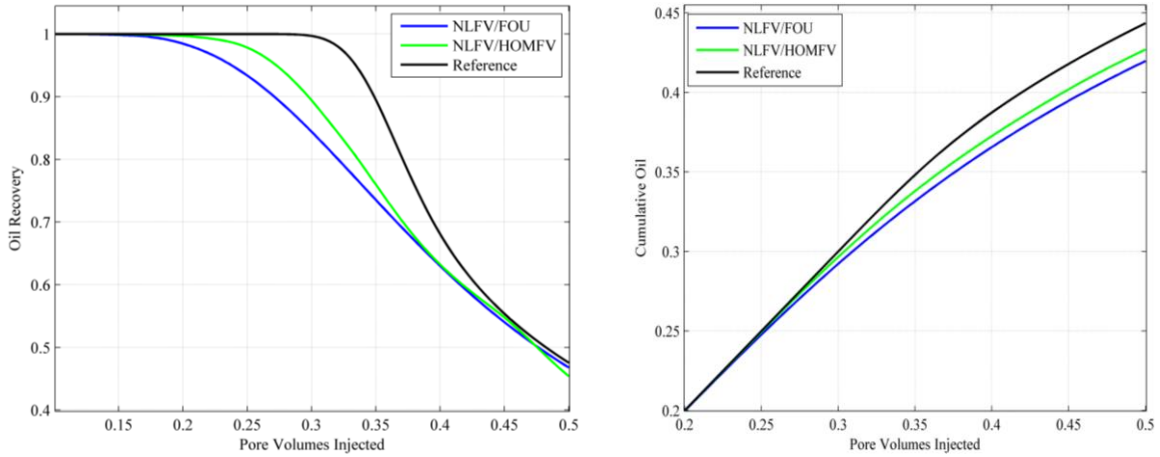

Figure 7. Results obtained for the ¼ of five spot problem in a homogeneous and anisotropic reservoir with a distorted quadrilateral mesh: recovered oil (left); cumulative oil (right).

5 CONCLUSION

In this paper, we have described a cell-centered non-linear finite volume method to simulate the displacement of oil by water in heterogeneous and anisotropic petroleum reservoirs. In order to discretize the elliptic pressure equation we use a non-linear finite volume formulation that satisfies the linearity-preserving criterion and produces monotone discrete solution even with interpolation weights negatives. To discretize the hyperbolic saturation equation we used a higher order MUSCL-type finite volume scheme based in a least squares gradient reconstruction with a proper slope limiting strategy in order to guarantee monotonicity. The formulation can be used in any polygonal grid. Representative model examples were used to prove the effectiveness of the method, and improved results are obtained when using higher-order scheme when compared to the classical FOU method, as expected. In the near future, we intend to investigate a truly multidimensional high-order discretization method for the

saturation equation over any polygonal grid and to evaluate the use of a Newton type method to solve the non-linear system of equations associated to the pressure solver.

ACKNOWLEDGEMENTS

The authors would like to thank the following Brazilian research agencies: Pernambuco State Foundation for Science and Technology (FACEPE), Brazilian National Counsel of Technological and scientific Development (CNPq), CENPES-PETROBRAS (SIGER - the Petrobras Network on Simulation and Management of Petroleum Reservoirs).

REFERENCES

Aavatsmark, I., 2002. An introduction to multipoint flux approximations for quadrilateral grids, *Comp. Geosciences*, 6: 405–432.

Lamine, S., Edwards, GM., 2010. Multidimensional upwind convection schemes for flow in porous media on structured and unstructured quadrilateral grids. *J Comput Appl Math,* 234:2106-2117.

Le Potier, C.,2005. Schema volumes finis monotone pour des operateurs de diffusion fortement anisotropies sur des millages de triangle nonstructures, *C. C. Acad. Sci, Paris*, I341: 787-792.

Lipnikov, K., Shashkov, M., Svyastskiy, D. & Vassilevski, Y., 2007. Monotone finite volume schemes for diffusion equations on unstructured triangular and shape-regular polygonal meshes. *Journal of Computational Physics,* 227(1):492-512.

Sheng, Z. & Yuan, G., 2011. The finite volume scheme preserving extremum principle for diffusion equations on polygonal meshes. *Journal of Computational Physics*, *230*(7):2588-2604.

Gao, Z. & Wu, J., 2010. A linearity-preserving cell-centered scheme for the heterogeneous and anisotropic diffusion equations on general meshes. *International Journal Numerical Method Fluids,* 67:2157-2183.

Gao, Z. & Wu, J., 2013. A small stencil and extremum-preserving scheme for anisotropic diffusion on arbitrary 2D and 3D meshes. *Journal of Computational Physics,* 250,308-331.

Wu, J. & Gao, Z., 2014. Interpolation-based second-order monotone finite volume schemes for anisotropic diffusion equations on general grids. *Journal of Computational Physics*, 275: 569-588.

Gao, Z. & Wu, J., 2015. A Second-Order Positivity-Preserving Finite Volume Scheme for Diffusion Equations on General Meshes." *SIAM Journal on Scientific Computing,* 37(1): A420-A438.

Agelas, L., Eymard, R. & Herbin, R., 2009. A nine point finite volume scheme for the simulation of diffusion in heterogeneous media, C.R. Acad. Sci. Paris Ser, 347:673-676.

Lönher, R., 2008. Applied computational fluid dynamics techniques: an introduction based on finite element methods. John Wiley & Sons.

Hirsch, C., 2007. Numerical Computation of Internal and External Flows: The Fundamentals of Computational Fluid Dynamics, Butterworth-Heinemann, vol. 1.

Blazek, J., 2001. Computational Fluid Dynamics: Principles and Applications. Elsevier.

Woodfield, PL., Kenjiro, S. & Kazuyoshi, N., 2004. A simple strategy for constructing bounded convection schemes for unstructured grids. *Int J Numer Meth Fl*, 46:1007-1024.

Herbin, R. & Hubert, R., 2008. Benchmark on discretization scheme for anisotropic diffusion problems on general grids, in: *Finite Volumes for Complex Applications V-Problems V*. Wiley, pp. 659-692.

Queiroz, LES., Souza, MRA., Contreras, FRL., Lyra, PRM. & Carvalho, DKE. 2014. On the accuracy of a nonlinear finite volume method for the solution of diffusion problems using different interpolations strategies. *Int J Numer Meth Fl*, 74(4):270-291.

Carvalho, DKE., Willmerdof, RB., Lyra, PRM., 2006. A node-centered finite volume formulation for the solution of two-phase flows in non-homogeneous porous media. *Int J Numer Meth Fl*, 53:1179-1219.

Aziz, K., 1979. Settare A. *Petroleum Reservoir Simulation*. New York.

Blasek, J., 2001. *Computational Fluid Dynamics: Principles and Applications*. Elsevier.